Analytical investigation of disturbance of seabed-sampled soil specimens and its influence on unconfined strength

Sugiyama, Yuri
Tachibana, Shinya
Sakaguchi, Hide
Iizuka, Atsushi

(Citation)
Soils and Foundations,58(3):689-701

(Issue Date)
2018-06

(Resource Type)
journal article

(Version)
Version of Record

(URL)
https://hdl.handle.net/20.500.14094/90007249

HOSTED BY
ELSEVIER
Available online at www.sciencedirect.com
ScienceDirect
Soils and Foundations 58 (2018) 689–701
SOILS AND FOUNDATIONS
www.elsevier.com/locate/sandf

Analytical investigation of disturbance of seabed-sampled soil specimens and its influence on unconfined strength

Yuri Sugiyama [a,*], Shinya Tachibana [c], Hide Sakaguchi [b], Atsushi Iizuka [c]

[a] *Port and Airport Research Institute, Yokosuka, Japan*
[b] *Doctor of Engineering, JAMSTEC, Japan*
[c] *Doctor of Engineering, Kobe University, Japan*

Received 16 January 2017; received in revised form 1 February 2018; accepted 27 February 2018
Available online 7 May 2018

Abstract

In view of the need to utilize ocean space and to develop seabed resources, the assessment of the stability of deep seabed soil has emerged as an important challenge in the field of geomechanics. To study seabed stability, the strength and stiffness of the natural ground must be ascertained. Accordingly, it is necessary either to conduct laboratory testing on soil specimens sampled from the seabed or to estimate the strength and stiffness by in-situ tests. While in the future it may be reasonable to conduct in-situ tests to estimate the stiffness and strength of seabed soil, it will still be necessary to compare the physical properties measured by in-situ testing with those measured by laboratory testing in advance of these determinations. In short, soil specimens must be sampled from the actual deep seabed, and laboratory mechanical tests must be conducted on the sampled soil specimens. However, soil sampled from the ocean bottom is subject to effects that differ from those exerted on soil sampled from the earth. More specifically, the non-negligible effects of disturbance are expected with soil sampled from the ocean bottom. The effects of disturbance occur during the sampling process due to the vaporization of dissolved gases, as these soil specimens are under relatively higher pressure and contain pore water with a high amount of dissolved gases. Therefore, numerical simulations were conducted in the present study to investigate the effects of vaporized dissolved gases on the mechanical behavior of soil specimens during sampling and on the undrained shear strength as determined by laboratory tests. The analyses revealed that the combination of the decreasing effective stress caused by the sampling and factors such as overconsolidation and unsaturation is attributable to the difference between the soil strength ascertained by laboratory testing and the in-situ soil strength.

Keywords: Disturbance; Marine clay; Unsaturated soil; Numerical simulation; Henry's law; Unconfined undrained test

1. Introduction

Since the discovery of methane hydrates (1930), cross-disciplinary scientific efforts have been directed towards clarifying the properties of deep seabed soil for the purpose of developing ocean seabed resources. Such efforts include Project Mohole (1961), the Deep Sea Drilling Project (DSDP, 1968), the International Phase of Ocean Drilling (IPOD, 1975), the Ocean Drilling Program (ODP, 1985), and the Integrated Ocean Drilling Program (IODP, 2003). However, in identifying the mechanical properties of deep seabed soil, it is difficult to ascertain the effects of the disturbance arising from the release of stress that specimens undergo during sampling. In this regard, pressure core sampling (Kubo et al., 2014) has been explored. However, this method lacks the theoretical basis to quantify the effects of the disturbance on specimens and remains at an undeveloped stage of understanding to interpret the test results. It has been pointed out that changes in the mechanical properties of sampled soil specimens are caused by the

Peer review under responsibility of The Japanese Geotechnical Society.
* Corresponding author.
E-mail address: sugiyama-yu@pari.go.jp (S. Yuri).

https://doi.org/10.1016/j.sandf.2018.02.026
0038-0806/

effects of the mechanical disturbance occurring during sampling or testing and of the disturbance arising from the release of stress. In these respects, the mechanical disturbance has been studied by Ladd and Lamb (1963) and Okumura (1969), followed by Tsuchida et al. (1988) and others (Mitachi et al., 2001; Tanaka and Tanaka, 1995). Similarly, Skempton and Sowa (1963) and Noorany and Seed (1965) were forerunners in terms of studies on the disturbance arising from the release of stress. Since then, researchers have worked to study the effect of changes in the effective stress of specimens resulting from the release of the confining pressure exerted on the undrained shear strength of specimens. This is a classic topic in geomechanics. Soil sampled from the deep seabed is unavoidably subject to the effects of mechanical disturbance, which remains to be reduced by developments in sampling technology. Even so, it is highly likely that the effects of the stress release after the removal of the high confinement pressure will continue to be a serious problem. Reported experiments have revealed the substantial effects of gases on the variation in momentary pressure in ordinary ground sediments (Tsui and Helfrich, 1983). Additionally, marine clay soil specimens sampled close to waterfront locations have exhibited residual effective stress measurements far smaller than those forecasted (Matsumoto et al., 1969) as well as measured degrees of saturation that decreased with depth (Fujishita, 1965). On the other hand, despite the fact that a residual effective stress larger than 98.1 kPa is apparently impossible in fully saturated soil, effective stress larger than 98.1 kPa has been measured in undisturbed samples collected from large depths (Watabe and Tsuchida, 2001). These findings have led to one of the most important problems in today's seabed soil surveys: the vaporization of dissolved gases that degrade the quality of the sampled specimens needed to ascertain the mechanical properties (Okusa, 1984). Recently, microscopic images of sampled specimens have illustrated that the gases were contained within the soil voids as small bubbles (Amaratunga and Grozic, 2009). This becomes a more serious problem with deep seabed soil. It is quite probable that soil from the deeper seafloor contains a larger amount of dissolved gases (Grozic et al., 2000; Kortekaas and Peuchen, 2008). In addition, sampling from such a deep ground involves substantial changes in pressure. Consequently, dissolved gases that vaporize due to these changes in pressure, which have not been accounted for at different water and seabed depths (i.e., depth below the seabed floor) in existing studies, are likely to exert an apparent effect.

The effects of the vaporization of dissolved gases can be explained by taking diver's disease as an example. Diver's disease, also known as "decompression sickness", or DCS, can be experienced by a diver after scuba diving. Nitrogen gas accounts for approximately 78% of air. Accordingly, when a diver uses an air cylinder, nitrogen gas dissolves into the diver's body. Larger amounts of nitrogen gas dissolve with increasing depths and increasing diving time. When a diver rises rapidly towards the sea surface at the end of the dive and the water pressure decreases, the dissolved nitrogen forms bubbles in the diver's body. The bubbles apply pressure on the nerves and joints of the diver, causing pain and abnormal sensations. This is the cause of diver's disease (Fig. 1). In the case of sampling specimens from the seabed, it is highly likely that phenomena similar to diver's disease will occur. During the process of sampling specimens from the seabed, large amounts of gases dissolved in the pore water of the saturated soil vaporize owing to the decreasing water pressure. Consequently, the soil becomes unsaturated (Fig. 2). This unsaturation process is thought to be one of the causes of the disturbance of sampled specimens, affecting changes in the effective stress. In recent years, the use of a pressure-conserving corer to maintain the in-situ water pressure during sampling has become possible. This method appears to be effective for preventing the vaporization of dissolved gases otherwise resulting from changes in pressure during sampling. However, this sampling method is immensely laborious and costly, making it difficult to sample many specimens. Therefore, it is necessary to propose an optimal test method for estimating the in-situ strength from sampled specimens by evaluating the disturbances in the specimens sampled by the conventional sampling technique. Okumura (1969a) used Boyle's law and Henry's law to theoretically calculate the effects exerted by gases contained in pore water on the residual effective stress of specimens. For this theoretical reasoning, Okumura used a total stress analysis to solve problems as well as coefficient B proposed by Skempton (1954) to estimate the residual effective stress. At the time of the study, many key ideas, such as the mechanics of unsaturated soil, were yet to be proposed. To ensure equilibrium, the total stress acting on a specimen was believed to equal the atmospheric pressure. However, the gas pressure produced by dissolved gases is not negligible; and therefore, researchers began to believe that the effective stress formula for saturated soil is incapable of predicting changes in effective stress in seabed soil (Esrig et al., 1977). It has become possible recently to explore the mechanical behavior of unsaturated soil due to a successful systemic arrangement of the mechanics of unsaturated soil and a soil/water/gas coupled analysis. On the basis of contemporary mechanics, it is not necessarily true that the pore gas pressure in a specimen is in equilibrium with the atmospheric pressure because, in actuality, suction occurs within the specimen. Thus, to examine the effects of dissolved gases on the quality degradation of sampled specimens, it is necessary to use the soil/water/gas coupled analysis. In this study, the pore gas pressure is expressed by the gauge pressure.

Given this situation, the purpose of the present study is to examine the effects of changes in the state of dissolved gases on the mechanical behavior of sampled specimens and on the undrained strength determined through laboratory testing. For this purpose, the study uses a mathematical model capable of representing changes in the state of dissolved gases and simulating sampling processes with increased precision. The analysis codes used in this study

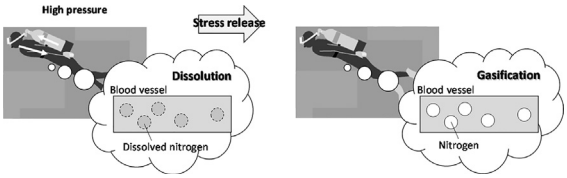

Fig. 1. Diver's disease.

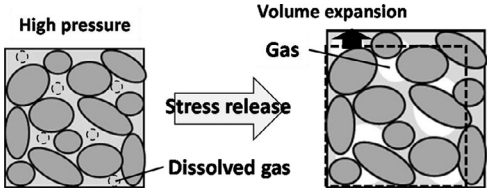

Fig. 2. Unsaturation process.

are given in the Appendix. Since the compressibility of seawater differs with the water depth (Dietrich, 1963), the expansion of pore water needs to be considered. However, the compressibility of pore water is much smaller than that of gas; and therefore, this study assumes that the expansion of pore water is negligible. Future needs, beyond the scope of this study, are to examine the effects of changes in temperature resulting from changes in the state of the dissolved gases, as well as the effects of the mechanical disturbance.

2. Simulation analysis of sampling and laboratory testing process

This section describes the analysis method and the selection of parameters used to simulate the process of sampling soil at various water/seabed depths. In addition, this section also describes the simulation of laboratory tests to examine the strength of the sampled specimens as determined through laboratory testing.

2.1. Simulation of sampling process

Cone penetration tests are often used as an in-situ test method to investigate the strength of the ocean floor ground (Oka et al., 2011; Nishio et al., 2009). The variation in the end resistance obtained from CPT test results is compared with the strength obtained from unconfined compression tests (Nishio et al., 2009). In the case of the land ground, which has been targeted so far, and the submarine ground, with a water depth of approximately 30 m, it has been found that the influence of the disturbance of the sample on the end resistance is small. However, in the case of the submarine ground with a deep water depth, laboratory tests using sampled specimens must be conducted since the influence of the disturbance accompanying the measurement of the end resistance is unknown. A piston core sampler is mainly used in ocean surveys, and soil specimens of the in-situ ground are sampled using a hollow tube called a core barrel (Matsumoto et al., 2009). The soil samples are collected by pressing the core barrel into the ground, lifting the sampler up to the land, and then pressing it out of the core barrel. Skempton and Sowa (1963) and Ladd and Lamb (1963) studied the effects exerted by possible disturbance on the changes in effective stress throughout the sampling process. Ladd and Lamb (1963) summarized the changes in effective stress over the whole sampling process, as shown in Fig. 3. In Fig. 3, the in-situ stress condition is represented by A. The overburden pressure is relieved as the borehole is bored. As this occurs, the state of effective stress migrates from point A to B through P. Furthermore, as the sampling tube is pressed into the ground and the specimen is lifted to the land, the state of effective stress shifts from B to C. Then, it shifts from C to D as the specimen is pressed out of the sampling tube, followed by the arrival at F through preservation and trimming. These are all changes in effective stress viewed from the perspective of the mechanical disturbance caused during sampling. Conventionally, it has been thought that no changes in effective stress would occur in response to the changes in pressure from B to C and when the total stress is relieved at D. However, it is highly probable that when dissolved gases vaporize, the specimen becomes unsaturated, and the changes in effective stress occur due to changes in pressure and the release of stress. Therefore, this study simulates the sampling process, dividing it into Process 1 and Process 2, which consider the vaporization of dissolved gases, as shown in Fig. 4. In Process 1, the focus is placed on the changes in stress resulting from the changes in pressure that would occur when a sampler is lifted. Process 1 corresponds to the process from B to C shown in Fig. 3. In Process 2, the focus is placed on the changes in stress resulting from the stress relief that takes place when the specimen is removed from the core barrel. Process 2 corresponds to the process from C to D shown in Fig. 3. In these two processes, it is assumed that the tested portions of the specimen would instantly be taken out, without regard to the mechanical disturbance arising at the time of the sampling and the trimming.

2.2. Simulation of laboratory tests

Subsequent to the simulation of the sampling process, the strength of the specimen disturbed by sampling is

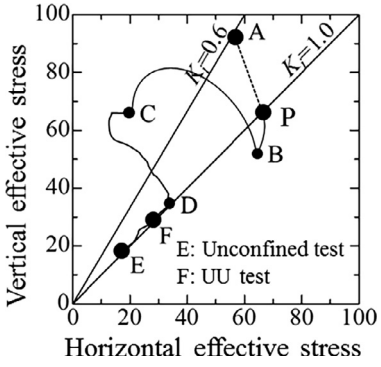

Fig. 3. Changes in effective stress during sampling (Ladd and Lamb, 1963).

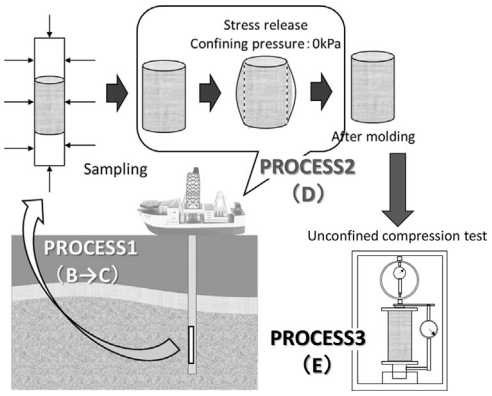

Fig. 4. Simulation of sampling process.

examined. Nakase (1967) demonstrated that many sliding failures on soft grounds in Japan have been successfully explained by assuming that half of the average of q_u, obtained through unconfined compression testing, equaled the undrained shear strength. Matsuo (1984) showed that a circular slip analysis, using the average of $q_u/2$, would make it possible to calculate the safety factor for the sliding failures studied by Nakase within the range of 0.9–1.1. These results have contributed to the notion that the use of the average of q_u to determine the strength of cohesive soil is valid in terms of engineering, resulting in its widespread use as a determination method (q_u method) for cohesive soil. In addition to unconfined compression testing, triaxial compression or triaxial expansion testing are methods for determining the strength of soil through laboratory analysis. In Japan, the unconfined compression test is commonly used as a method for measuring the strength of cohesive seabed soil, as mentioned above. It is used because the method has proven itself through many results, is simple to conduct, and is highly cost-effective. Therefore, this study employs the strength determined through the unconfined compression simulation, described as Process 3, for the purpose of a strength analysis (Fig. 4).

2.3. Setting initial stress and boundary conditions

Simulation analyses were conducted in this study assuming that specimens would be sampled at various water/seabed depths. Fig. 5 shows an example case of a water depth of 100 m and a seabed depth of 100 m. Without regard to the distribution of hydrostatic pressure in the core barrel, the initial pore water pressure in the tube was 2000 kPa (at the sampling depth). The amount of dissolved gases was taken as proportional to the pore gas pressure. Hence, assuming that dissolved gases in a saturated condition are present in pore water at the depth of 200 m, the initial pore gas pressure was set at 2000 kPa, the initial pore water pressure. In this process, the initial suction was 0.0 kPa and the degree of saturation was 1.0, as determined by the soil–water characteristic curve used in this study. When lifting the sampler to the sea surface, the top and bottom surfaces of the core barrel were in contact with seawater. Hence, it is

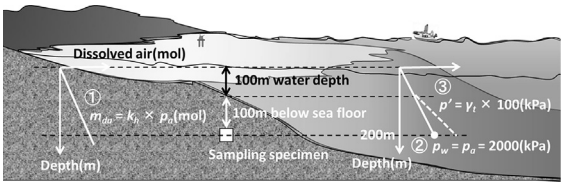

Fig. 5. Initial stress setting (water depth: 100 m; seabed depth: 100 mbsf).

highly likely that the soil present at the ends in a saturated condition was directly affected by the changes in water pressure during the lift. Thus, for Process 1, it was assumed that suction at the upper and lower end faces would be constantly 0, using the mesh diagram in Fig. 6(a), which represents a specimen in a core barrel with confined lateral deformation. In this process, the specimen was divided one-dimensionally into 100 elements, with each element measuring 0.01 m by 0.01 m. Fig. 7 shows the changes in pore water pressure, pore gas pressure, and suction at the upper and lower end faces that took place during the core barrel lifting process.

Existing studies report that specimens used in laboratory testing vary in strength by up to 50%, depending on the location in the thin-walled tube from which they had been taken (Tanaka et al., 1992; Hvorslev, 1949; Fujishita, 1965). This led us to conduct simulation analyses for Process 2, assuming that after Process 1, the residual confining pressure applied to each of the tube elements shown in Fig. 6(a) decreased to a confining pressure equal to 0 [Fig. 6(b)]. In Process 2, the element simulation has been carried out for each element used by the analysis in Process 1. This means that, in Process 2, 100 calculations

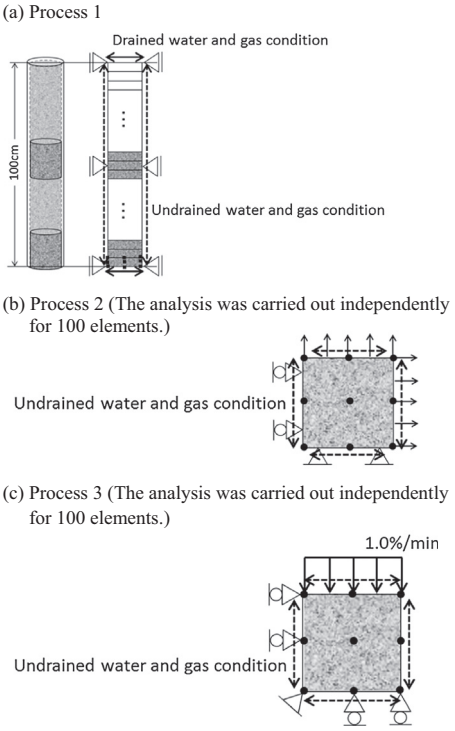

Fig. 6. Diagram of analysis mesh.

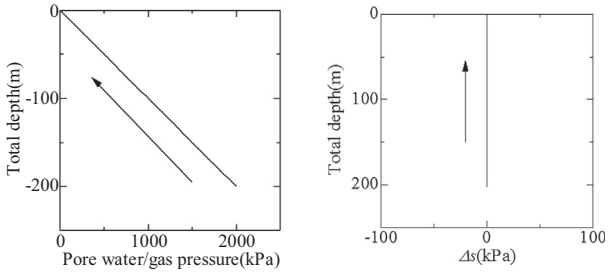

Fig. 7. Changes in pore water pressure, pore gas pressure, and suction at boundaries in Process 1.

were performed for each case performed in Process 1. This simulation imposed entirely both gas- and water-undrained boundary conditions. Following Process 2, unconfined compression simulations were conducted for each element under entirely both gas- and water-undrained conditions, as shown in Fig. 6(c) (Process 3). The specimen was sheared at a rate of 1.0%/min. To ensure that the simulation analysis handled Processes 1, 2, and 3 without interruption, all the initial conditions, including the void ratio and the degree of saturation for Processes 2 and 3, were set to be identical to the final conditions of Processes 1 and 2, respectively. In this study, it is assumed that samples can be instantaneously taken out from the core barrel; hence, both gas- and water-boundary conditions were set as the undrained condition in Process 2. Moreover, considering that the unconfined compression test has a high shear rate and the water permeability coefficient of submarine clay is low, it can be said that both gas- and water-boundary conditions were set as the undrained condition in Process 3.

2.4. Selecting analysis parameters

Table 1 lists the material parameters used in the analysis. The analysis assumed that the natural ground was highly uniform and homogenous in the direction of depth. The compression and swelling indexes that Tanizaki et al. (2005) obtained from the alluvial clay of Osaka Bay as laboratory test results were used because the mechanical properties of the deep seabed soil were unknown. Similarly, the values for the void ratio and the weight per unit volume were provisionally established based on measurement data of the alluvial clay ground of Osaka Bay (20 m in water depth and 0–20 m below sea floor (mbsf)) (Tsuchida et al., 1988). Estimating the soil–water characteristics of the seabed ground is difficult since it is considered to be in a saturated state and no water retention tests have been carried out. Hence, the hydraulic conductivity and the soil–water characteristic curve shown in Fig. 8 were based on an assumption that the specimen was cohesive soil (Kawazu et al., 2011). Henry's constant was determined using the dissolved-gas data obtained from the Sea of Okhotsk off Abashiri (Yamashita et al., 2013, 2014). Fig. 9 shows the concentrations of dissolved gases in the pore water. These data were obtained from soil at a water depth of 570–750 m and a seabed depth of 0.26–1.96 mbsf. Since the gas that dissolved in the water contained various gases, like carbon dioxide, methane, etc., as shown in Fig. 9, the authors assumed that the dissolved gas in the pore water was a mixed gas containing these gases. In the simulation, the initial stress state was set to a normal consolidation state. A hydrostatic state was assumed as the initial condition. The initial stress-induced anisotropy was not taken into consideration here.

Table 1
Initial stress conditions and analysis parameters.

Compression index λ	0.2173
Swelling index κ	0.0344
Initial void ratio e	1.0
Grain density G_s	2.71
Se-hardening model parameters a	10
n_s	1.2
Initial saturation S_r	1.0
EC model parameters n_E	1.5
Coefficient of permeability k_w (cm/s)	6.94E−04
Coefficient of air permeability k_a (cm/s)	6.94E−02
Amount of substance M_d (g/mol)	33.86
Gas constant R(J/K mol)	8.31
Temperature T(K)	275.15
Henry's law parameter k_h (g/kPa)	0.306

3. Mechanical behavior during sampling and effects of sampling on unconfined compression testing

Firstly, a simulation of the sampling process (Processes 1 and 2) was conducted with a soil/water coupled model,

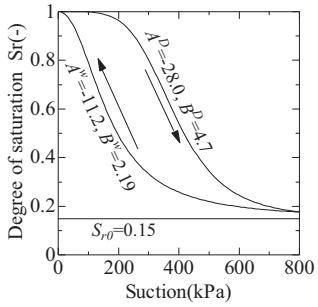

Fig. 8. Soil–water retention characteristic curves. Values for A and B : the fitting parameters used in Eq. (9), and the suffixes D and W indicate drying and wetting processes, respectively, Sr_0: critical degree of saturation.

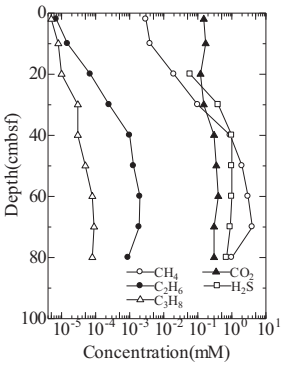

Fig. 9. Dissolved gases in pore water (Yamashita et al., 2013, 2014).

without considering the vaporization of dissolved gases, to represent sampling from a water depth of 1000 m and a seabed depth of 20 mbsf. Figs. 10 and 11 show the changes in pore water pressure and effective stress, respectively, for the elements at the center portion of the core barrel. The specimens initially in a fully saturated state remained consistently saturated even with changes in pressure (Process 1) and stress relief (Process 2). Consequently, the stress reduction could be entirely absorbed, as negative pressure, by the pore water pressure. Therefore, no changes took place in the effective stress from the initial state, as shown in Fig. 11. This implies that specimens from which the stress has been released will be fully undisturbed specimens. In this regard, similar trends were exhibited irrespective of the water depth, seabed depth, and position in the tube. Meanwhile, Figs. 12–14 show the results of a similar simulation analysis, which used a soil/water/gas coupled model that factored in the vaporization of dissolved gases. Fig. 12 shows the residual pore gas pressure, residual pore water pressure, and coefficient of earth pressure at rest after Process 1. This is the case for a water depth of 0 m (land surface soil). The term "seabed soil" is also used, for convenience, for denoting a water depth of 0 m. Both pore gas pressure and pore water pressure at both the upper and lower end surfaces were 0 kPa because they were given a hydraulic boundary, as shown in Fig. 7. From Fig. 12(a), it is seen that the pore water pressure in the tube becomes larger than 0 due to the vaporization of the dissolved gases. This is the same trend as seen in the results obtained by Fujishita (1965) using an actual sampled specimen. From Fig. 12(b), it is seen that the pore gas pressure in the tube

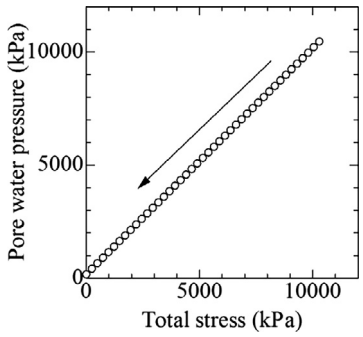

Fig. 10. Changes in pore water pressure.

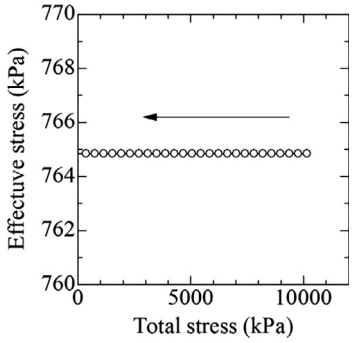

Fig. 11. Changes in effective stress.

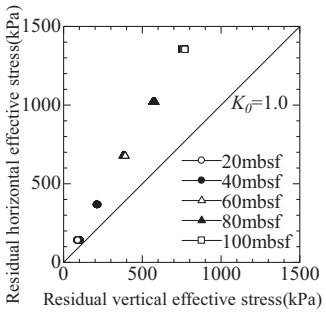

(a) Coefficient of earth pressure at rest

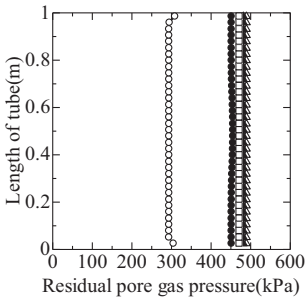

(b) Residual pore gas pressure

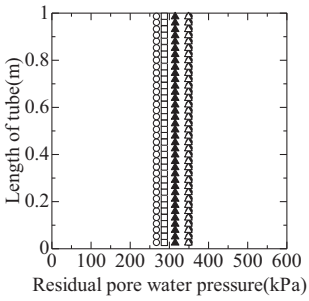

(c) Residual pore water pressure

Fig. 12. Coefficient of earth pressure at rest, residual pore gas pressure, and residual pore water pressure after Process1 (Water depth: 0 m).

does not become equal to the absolute pressure. Moreover, since the tube constrained the lateral deformation, the sample in the tube was in an anisotropic stress state after Process 1. However, the degree of anisotropy did not change within the tube. Figs. 13 and 14 summarize the distribution of the residual degree of saturation and the residual effective stress ratio in the specimens present in the tube after Process 1. The residual effective stress ratio is obtained by dividing the residual effective stress after Process 1 ($p'res$) by the in-situ effective stress ($p'i$). The residual degree of saturation means the degree of saturation after the simulation of the sampling. These results were obtained by modeling a sampling at seabed depth intervals of 20 mbsf up to 100 mbsf and at water depths of 200 m and 400 m. A similar simulation analysis was conducted, for comparison purposes, assuming a case of a water depth of 0 m. Fig. 13 shows that, in all cases, unsaturation occurred in the specimens in the tube as a result of the vaporization of the dissolved gases induced by changes in pressure. The differences in the distribution of the degree of saturation in the specimens in the

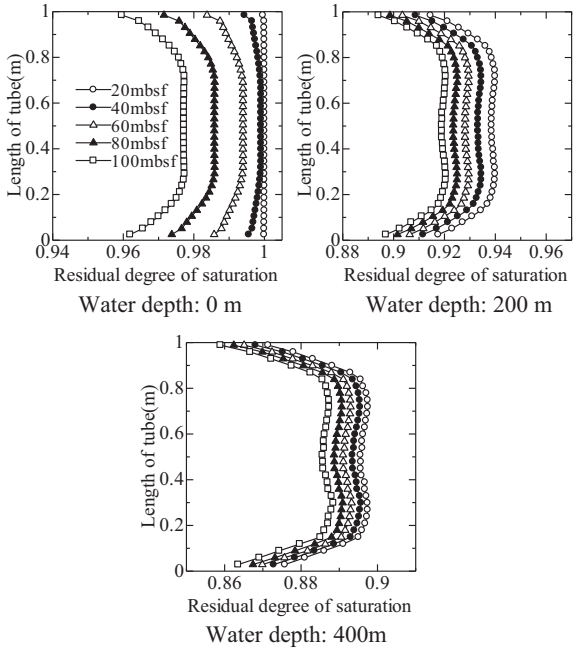

Fig. 13. Distributions of residual degree of saturation in the tube.

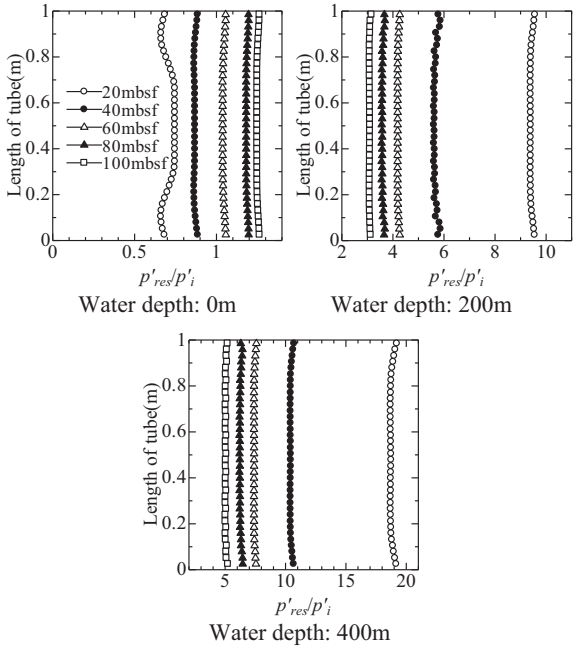

Fig. 14. Distributions of residual effective stress ratios in the tube.

tube are attributable to the fact that the varying seabed depths were smaller with the increasing water depth. The residual effective stress was not equal to the in-situ overburden pressure because the unsaturation of the sampled specimens resulted in changes in the effective stress (Fig. 14). In the case of a water depth of 0 m, the residual effective stress was smaller than the in-situ overburden pressure with a decreasing seabed depth, as shown in Fig. 14. In the case of water depths below 200 m, the residual effective stress tended to be greater than the in-situ overburden pressure with an increasing seabed depth.

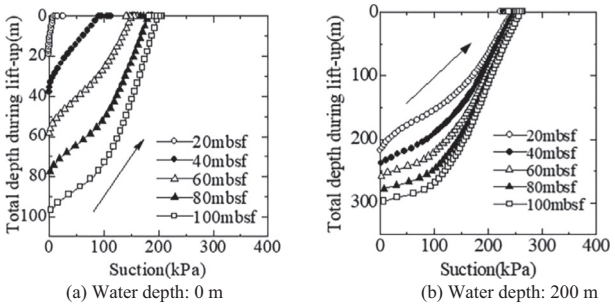

Fig. 15. Total water depth vs. suction.

To investigate the reason for the different trends, Fig. 15 summarizes the changes in suction that occurred at the 0.5 m position (center) in the tube during the lifting process (Process 1). Fig. 15 shows the 0- and 200-m water depth cases. Only these two cases are illustrated because the distributions of residual effective stress showed similar trends at water depths of 200 m and deeper. For the 0-m water depth case, Fig. 15(a) reveals larger increments in suction with increasing seabed depth. In contrast, in the 200-m water depth case [Fig. 15(b)], the increments in suction remained approximately uniform irrespective of the seabed depth. Meanwhile, it is known that a tendency towards unsaturation is more noticeable with an increasing seabed depth, independent of the water depth. These results suggest that different trends in the residual effective stress ratio occur depending on the water depth due to the equilibrium between changes in suction and changes in the degree of saturation.

As an effect of unsaturation, the pore water pressure and pore gas pressure inside the tube became higher than those at the upper and lower ends of the tube, generating a hydraulic gradient in the tube. For this reason, after being lifted, the tube was left to stand for a sufficient period of time until the stress state had stabilized. For this period, the water head and the gas pressure head between the upper and lower ends of the tube were assumed to be constant at 0. Fig. 15 reveals the change in suction at a water depth of 0 m that occurred during the stabilization period. For the case of the 400-m water depth and the 100-m seabed depth, unsaturation was the most noticeable. Fig. 16 shows the distributions of suction and degree of

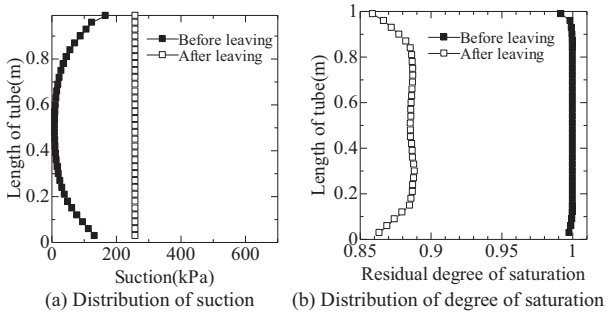

Fig. 16. Distributions of suction and residual degree of saturation in the tube (water depth: 400 m; seabed depth: 100 m).

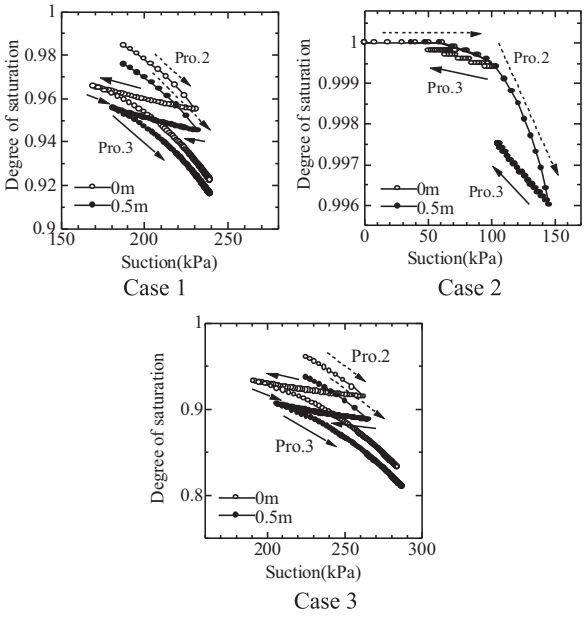

Fig. 17. Suction vs. degree of saturation.

saturation before and after the stabilization period. Fig. 16 (a) & (b) reveal that during the stabilization period, the distribution of suction became uniform throughout the tube, while the degree of saturation became non-uniform in the tube. Different soil–water characteristic histories that developed at different positions in the lifted tube caused these different trends. The results suggest that the degree of saturation becomes non-uniform even after the stabilization of suction in the tube because the changes in pressure during the process of the lifting of the tube influence the changes in stress in the sampled specimen. Additionally, this non-uniformity is caused by different stress change histories that develop at different positions in the tube during the lifting process.

Next, this study investigated the mechanical behavior that took place in Processes 2 and 3. Changes in suction and the degree of saturation in these processes are summarized in Fig. 17. Case 1 shows the results of an analysis simulating sampling from a water depth of 0 m and a seabed depth of 20 mbsf. Cases 2 and 3 show the results of simulations at a water depth of 0 m and a seabed depth of 100 m and at a water depth of 200 m and a seabed depth of 20 m, respectively. Due to the occurrence of the stress state variation in the core barrel after Process 1, each case shows the results for elements located at the 0.5 m (center) position and at the 0 m (end) position of the tube. A comparison of Cases 1 and 2 reveals that, even at the same water depth, unsaturation occurred more noticeably before Process 2 and suction increased to a greater degree with an increasing seabed depth. A comparison of Cases 1 and 3 reveals that approximately the same level of change occurred in the degree of saturation during Process 2 independent of the water depth. However, the degree of saturation after sampling decreased with the increasing water depth because the specimen in Process 1 became unsaturated to a greater degree with an increasing water depth. In each case, when a comparison was made with regard to the differences arising from different positions in the core barrel, the specimens exhibited the same trend in mechanical behavior in Processes 2 and 3, independent of the positions in the tube. Nevertheless, the closer to either tube end position, the more noticeable the changes in the degree of saturation during the sampling process. During Process 3, the degree of saturation increased during shearing and the degree of saturation decreased in the middle of shearing only at the tube ends for Case 1. These changes in the degree of saturation that occurred during shearing were more noticeable in Cases 2 and 3, representing greater seabed and water depths.

Fig. 18 shows the changes in confining pressure, and the time–stress and time–pressure profiles in the tube during Process 2. This is the case of a water depth of 200 m and a seabed depth of 20 m. In Process 2, the calculation was continued while keeping the horizontal and vertical confining pressure at 0 until the stress after unloading did not change. From Fig. 18(a), it is seen that the specimen that was in the anisotropic state after Process 1 became isotropic. This is because the confining pressure equaled the atmospheric pressure. The effective stress, pore gas pressure, and pore water pressure decreased with unloading, as shown in Fig. 18(b)–(d). These results reveal that the sampled specimens became overconsolidated due to the decreasing effective stress. Fig. 19 shows the effective stress paths in Processes 2 and 3, and each case shows the results for the elements located at the 0.5-m (center) position and the 0-m (end) position of the tube. These simulations were conducted for each element under entirely gas- and water-undrained conditions. In Fig. 19, the dashed lines indicate the results of a shearing simulation of the natural ground.

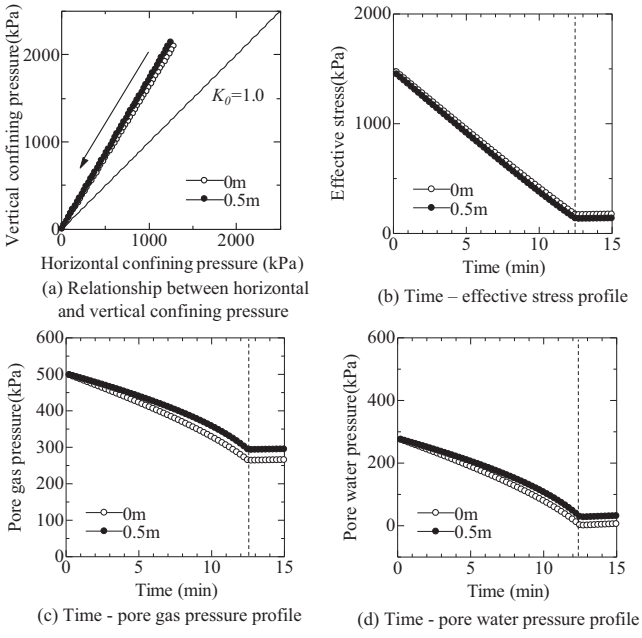

Fig. 18. Changes in confining pressure, time-stress, and time-pressure profiles in the tube during Process 2 (Water depth: 200 m, Seabed depth: 20 mbsf).

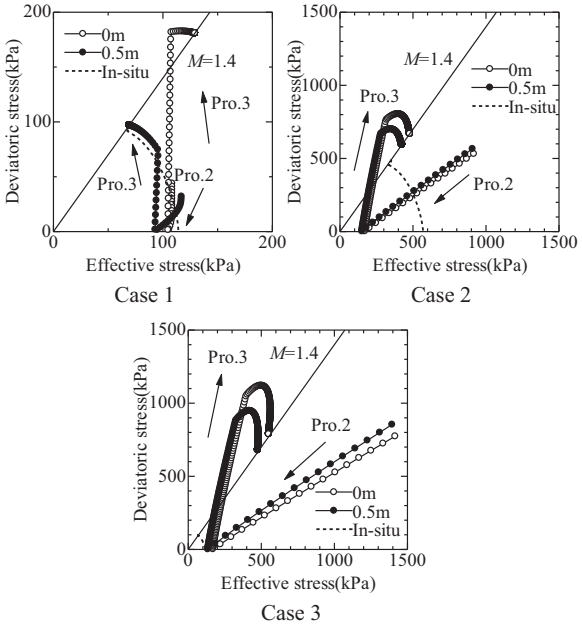

Fig. 19. Effective stress paths.

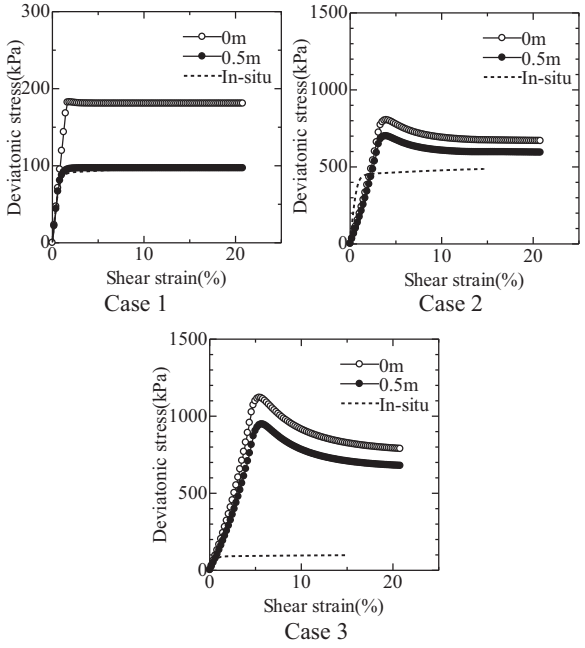

Fig. 20. Stress vs. strain.

Fig. 19 reveals that, in all cases, after Process 2, the effective stress became lower than the in-situ overburden pressure, and the sampled specimens became overconsolidated. The degree of overconsolidation was greater with increasing water and seabed depths. This was caused by the increasing suction in Process 1, which induced a higher effective stress than the in-situ overburden pressure. This, in turn, raised the pre-consolidation pressure. In Cases 2 and 3, in which noticeable overconsolidation occurred in Process 2, strength degradation developed during shearing. The lowered degree of saturation resulting from volume expansion in this process is thought to have caused the changes in the degree of saturation in Process 3, as shown in Fig. 17. Additionally, Fig. 20 shows the stress–strain relationships exhibited in Process 3. These results illustrate that in Cases 2 and 3, the peak strength was apparent due to the increasing overconsolidation ratio.

4. Distribution of unconfined strength

Fig. 21 summarizes the distributions of unconfined strength at various water depths. These analysis results reveal that our analysis overestimated the in-situ strength at most depths. The mechanical disturbance can decrease a specimen's strength by several tens of a percent (Okumura, 1969b). Considering a decrease in strength of several tens of a percent, the strength suggested by our analysis results became smaller, while the maximum strength still remained larger than the in-situ strength. In the 0-m water depth case, the unconfined strength of the specimens sampled from seabed depths shallower than 50 mbsf was similar to the in-situ strength. At depths of approximately 30 mbsf, the mean strength value between the minimum and the maximum was similar to the in-situ

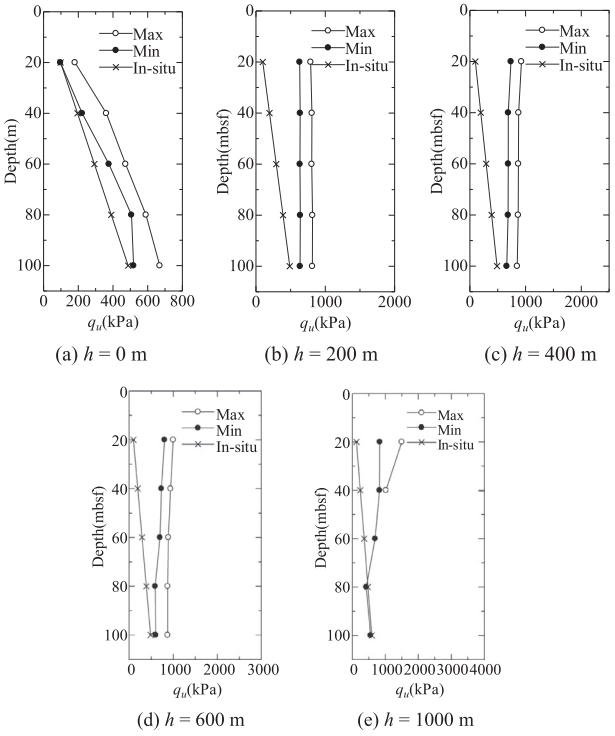

Fig. 21. Distributions of unconfined strength at various water depths.

strength, even with the mechanical disturbance taken into account. Tsuchida et al. (1988) demonstrated that the q_u method was a proven method up to depths of 25–30 mbsf. This is consistent with our analysis results and it can be interpreted as indicating that the approximate in-situ strength can be determined if a state of equilibrium is achieved between the decreasing effective stress resulting

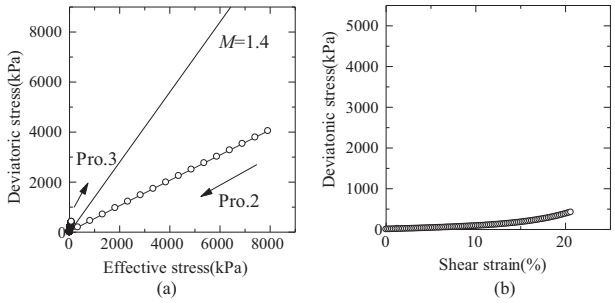

Fig. 22. Stress paths and stress vs. strain for specimen at the 0.98 m position in core barrel from seabed depth of 80 mbsf and water depth of 1000 m

from the stress relief during sampling and the effects exerted on the strength by unsaturation, which result from the changes in pressure or confinement pressure and from overconsolidation. Fig. 22 shows that the testing of the specimens sampled at water depths of 200 m or more resulted in a nearly constant strength, independent of the overburden pressure. Furthermore, the specimens obtained at water depths of 200–600 m exhibited almost the same level of strength. For the water depth of 1000 m, the minimum strength equaled the in-situ strength if the specimens were taken from a deep part of the seabed. Given this information, Fig. 21 shows an effective stress path and a stress–strain curve obtained in Process 3 for the case of a water depth of 1000 m and a seabed depth of 80 m. The results shown in Fig. 22 were obtained for the element that marked the minimum strength. Fig. 22(a) reveals that the initial effective stress is very low (10 kPa) before shearing. Moreover, the overconsolidation ratio of the specimen is very large. This result is interpreted as follows. The very low initial effective stress led to low shearing rigidity and the relatively slow development of strength, as shown in Fig. 22(b). In fact, the specimens failed to exhibit the peak strength until the shear strain reached 20%, which resulted in the specimens presenting low strength. It should be noted that Fig. 22(b) does not plot the maximum strength for the water depth of 1000 m. This is because the maximum strength was too high to plot for seabed depths greater than 40 mbsf at that water depth. These results suggest that the strength determined through unconfined compression testing depends on the decreasing effective stress and the degrees of unsaturation and overconsolidation. Furthermore, when a state of equilibrium is achieved between these factors, the determined strength equals the in-situ strength. However, at greater water depths, these factors tend to not be in equilibrium. In summation, the unconfined compression testing method may not be suitable for estimating the stability of the deep seabed ground.

5. Conclusion

By simulating the sampling process, we investigated the effects of changes in the state of dissolved gases on the mechanical behavior of sampled specimens and on the undrained shear strength determined through laboratory testing. The investigation results revealed that the vaporization of dissolved gases has substantial effects on the changes in stress in the sampled specimens, and that the undrained strength of the sampled specimens determined through unconfined compression testing can lead to erroneous estimations of the in-situ strength. The effects of the vaporization of dissolved gases on the undrained strength are more noticeable with increasing water and seabed depths; and hence, it may be inappropriate to use the results of unconfined compression testing to ascertain the in-situ strength of deep seabed soil. However, the determined strength becomes equal to the in-situ strength if the effects of overconsolidation and desaturation on the strengthening and the effects of the decreasing effective stress and the shearing rigidity on the strength degradation are balanced. Nevertheless, these factors tended to be out of equilibrium with increasing water and seabed depths, leading to erroneous soil strength estimations.

For the envisioned future growth of seabed development, a basic and essential requirement is to assess the stability of seabed soil. Without the accurate ascertainment of the in-situ strength, it is impossible to promote seabed development. Using the pressure-temperature reserved sampling method, samples can be collected while minimizing the disturbance. However, this sampling method is very costly, and thus, the sampling sites are limited. When uneven ground is distributed, like in Japan, as many samples as possible need to be collected. In this study, even if the influence of the disturbance is large, the strength could be estimated by considering the effect of suction caused by the sea water and seabed depths.

Appendix A

The analysis codes used in this study are summarized below. For details, refer to Sugiyama et al. (2016).

A.1. Continuity equations

The mixture theory is used to model the soil materials as a multiphase mixture. It is assumed that the equation of state for ideal gas and Henry's law are applicable for the gas-phase gas that exists in the voids among soil particles and for dissolved gas, respectively. For undissolved gas, the following equations are derived from the equation of state for an ideal gas to express gaseous density:

$$p_g V_g = \frac{m_g}{M^*} R^* T \tag{1a}$$

$$\rho_g = \frac{m_g}{V_g} = \frac{p_g M^*}{R^* T} \tag{1b}$$

$$\bar{\rho}_g = \frac{m_g}{V} = n(1 - S_r)\frac{p_g M^*}{R^* T} \tag{1c}$$

where ρ_g: true mass density of gas; $\bar{\rho}_g$: partial mass density of gas; m_g: mass of gas; V_g: volume of gas; R^*: gas constant

(an equivalent value for unit conversion); M^*: amount of substance determined through unit conversion; T: absolute temperature; and p_g: gas pressure. According to Henry's law, the density of the gas dissolved into the liquid phase is determined, as follows:

$$m_{dg} = k_h p_g V_w \tag{2a}$$

$$\rho_{dg} = \frac{m_{gd}}{V_w} = k_h p_g \tag{2b}$$

$$\bar{\rho}_{dg} = \frac{m_{dg}}{V} = nS_r k_h p_g \tag{2c}$$

where ρ_{dg}: true mass density of dissolved gas; $\bar{\rho}_{dg}$: partial mass density of dissolved gas; m_{dg}: mass of dissolved gas; V_w: volume of the liquid phase; and k_h: Henry's constant.

The law of conservation of mass for solid, liquid, and gas phases (including dissolved gases) is expressed as follows. Subscript α is used to distinguish the variables of the phases: $\alpha = s, w, g, dg$.

$$\dot{\bar{\rho}}_\alpha + \bar{\rho}_\alpha \mathrm{div}\boldsymbol{v}_\alpha = 0 \ (\bar{\rho}_\alpha = \phi_\alpha \rho_\alpha) \tag{3}$$

where $\bar{\rho}_\alpha$: partial mass density; ρ_α: true mass density; $\boldsymbol{v}_\alpha$: actual velocity of phase; and ϕ_α: volume occupancy. The dot denotes an increment. The following continuity equation for the liquid phase is derived from the laws of mass conservation for solid and liquid phases:

$$\dot{n}S_r\rho_w + n\dot{S}_r\rho_w + nS_r\rho_w \mathrm{div}\boldsymbol{v}_w = 0 \tag{4}$$

where n: porosity and S_r: degree of saturation. The following continuity equation is obtained from the law of conservation of mass for solid and gas phases, as well as Eqs. (1c) and (2c):

$$-(1-S_r)\dot{\varepsilon}_v - n\dot{S}_r + \frac{n(1-S_r)}{p_\varepsilon}\dot{p}_g + \mathrm{div}\boldsymbol{v}_g - \frac{S_r k_h p_g}{\rho_g}\dot{\varepsilon}_v + \frac{nk_h p_g}{\rho_g}\dot{S}_r + \frac{nS_r k_h}{\rho_g}\dot{\rho}_g + \frac{k_h p_g}{\rho_g}\mathrm{div}\boldsymbol{v}_w = 0 \tag{5}$$

The migration of gas and water is expressed by the following equations, assuming that Darcy's law is applicable:

$$\tilde{\boldsymbol{v}}_{\boldsymbol{w}} = -k_w k_{rw} \cdot \mathrm{grad}h \tag{6a}$$

$$\tilde{\boldsymbol{v}}_{\boldsymbol{g}} = -k_g k_{rg} \cdot \mathrm{grad}h_g \tag{6b}$$

$$h_g = \frac{p_g}{\rho_w g} \tag{6c}$$

$$k_{rw} = S_e^{1/2}\left[1-(1-S_e^{1/m})^m\right]^2 \tag{6d}$$

$$k_{rg} = (1-S_e)^{1/2}(1-S_e^{1/m})^{2m} \tag{6e}$$

$$S_e = \frac{S_r - S_{rc}}{1-S_{rc}} \tag{6f}$$

where $\tilde{\boldsymbol{v}}_{\boldsymbol{w}}$: relative velocity of the liquid phase to the solid phase; $\tilde{\boldsymbol{v}}_{\boldsymbol{g}}$: relative velocity of the gas phase to the solid phase; ε_v: volumetric strain of soil; p_g: pore gas pressure; k_w: saturated hydraulic conductivity; k_{rw}: specific hydraulic conductivity; h: total head; h_g: gas pressure head; S_e: effective degree of saturation; S_{rc}: critical degree of saturation; and m: Mualem's coefficient (Mualem, 1976). Eqs. (6d) and (6e) represent the specific hydraulic conductivity proposed by van Genuchten (1980).

A.2. Constitutive model and soil–water characteristic curves

For the constitutive model for unsaturated soil, this study uses the model proposed by Ohno et al. (2007). The effective stresses are expressed by the following equations:

$$\boldsymbol{\sigma}' = \boldsymbol{\sigma}_{\mathbf{net}} + p_s\mathbf{1} = \boldsymbol{\sigma}_{\mathbf{net}} + S_e s\mathbf{1} \tag{7a}$$

$$\boldsymbol{\sigma}_{\mathbf{net}} = \boldsymbol{\sigma}^{\mathbf{T}} - p_g\mathbf{1} \tag{7b}$$

$$s = p_g - p_w \tag{7c}$$

where $\boldsymbol{\sigma}'$: effective stress tensor; $\boldsymbol{\sigma}_{\mathbf{net}}$: net stress tensor; p_s: suction stress; $\mathbf{1}$: second order unit tensor; s: suction; $\boldsymbol{\sigma}^{\mathbf{T}}$: total stress tensor; and p_w: pore water pressure. The effective stress expressed by Eq. (7a) reduces to Terzaghi's effective stress under saturated conditions. The yield function is defined by the following equations:

$$f(\boldsymbol{\sigma}', \zeta, \varepsilon_v^p) = MD\ln\frac{p'}{\zeta p'_{sat}} + D\frac{q}{p'} - \varepsilon_v^p = 0 \tag{8a}$$

$$\zeta = \exp\left[(1-S_e)^{n_s}\ln a\right] \tag{8b}$$

$$MD = \frac{\lambda-\kappa}{1+e_0} \tag{8c}$$

$$p' = \frac{1}{3}\boldsymbol{\sigma}' : \mathbf{1} \tag{8d}$$

$$q = \sqrt{\frac{3}{2}\boldsymbol{\sigma}_{\mathbf{D}} : \boldsymbol{\sigma}_{\mathbf{D}}} \tag{8e}$$

$$\boldsymbol{\sigma}_{\mathbf{D}} = \boldsymbol{\sigma}' - p'\mathbf{1} \tag{8f}$$

where ε_v^p: plastic volumetric strain; M: critical stress ratio expressed in terms of q/p'; D: dilatancy coefficient; a and n_s: parameters representing increases in yield stress resulting from an unsaturated condition; λ: compression index; κ: swelling index; $\boldsymbol{\sigma}_{\mathbf{D}}$: deviator stress tensor; e_0: void ratio at the yield point; and p'_{sat}: yield stress at a perfectly saturated condition.

Assuming that the current stress is constantly on the yield surface, the consistency condition is expressed as follows:

$$\dot{f}(\boldsymbol{\sigma}', S_e, \varepsilon_v^p) = \frac{\partial f}{\partial \boldsymbol{\sigma}'} : \dot{\boldsymbol{\sigma}}' + \frac{\partial f}{\partial S_e}\dot{S}_e + \frac{\partial f}{\partial \varepsilon_v^p}\dot{\varepsilon}_v^p = 0 \tag{9}$$

The nonlinear elastic constitutive model is described as

$$\dot{\boldsymbol{\sigma}}' = \boldsymbol{C}^e : \dot{\boldsymbol{\varepsilon}}^e + K^{S_e}\mathbf{1}\dot{S}_e \tag{10}$$

Note that in this equation,

$$\boldsymbol{C}^e = K\mathbf{1}\otimes\mathbf{1} + 2G\mathbf{A}$$

$$G = \frac{3(1-2\nu')}{2(1+\nu')}K$$

$$K = \frac{1+e_0}{\kappa}p'$$

$$K^{S_e} = n_s p' \ln a(1-S_e)^{n_s-1}$$

where G is the elastic shear modulus, ν' is Poisson's ratio, K is the elastic bulk modulus, and K^{S_e} is the elastic bulk modulus associated with the degree of saturation.

The rate of plastic strain $\dot{\boldsymbol{\varepsilon}}^p$ is assumed to follow the associated flow rule as follows:

$$\dot{\boldsymbol{\varepsilon}}^p = \gamma \frac{\partial f}{\partial \boldsymbol{\sigma}'} \tag{11}$$

where γ is the plastic multiplier. Next, on the assumption that the rate of strain is composed of elastic and plastic components, the following equation holds:

$$\dot{\boldsymbol{\varepsilon}} = \dot{\boldsymbol{\varepsilon}}^e + \dot{\boldsymbol{\varepsilon}}^p \tag{12}$$

By determining plastic multiplier γ from Eqs. (9)–(12) and substituting the results into Eq. (10), we obtain

$$\dot{\boldsymbol{\sigma}}' = \boldsymbol{C} : \dot{\boldsymbol{\varepsilon}} - \boldsymbol{D}\dot{S}_e \tag{13}$$

This is a constitutive equation that takes desaturation into account. For this equation, the following holds:

$$\boldsymbol{C} = \boldsymbol{C}^e - \frac{\boldsymbol{C}^e : \frac{\partial f}{\partial \boldsymbol{\sigma}'} \otimes \frac{\partial f}{\partial \boldsymbol{\sigma}'} : \boldsymbol{C}^e}{\frac{\partial f}{\partial \boldsymbol{\sigma}'} : \boldsymbol{C}^e : \frac{\partial f}{\partial \boldsymbol{\sigma}'} - \frac{\partial f}{\partial \varepsilon_v^p}\frac{\partial f}{\partial p'}}$$

$$\boldsymbol{D} = \frac{\boldsymbol{C}^e \frac{\partial f}{\partial \sigma'_{kl}}\left(\frac{\partial f}{\partial p'}K^{S_e} + \frac{\partial f}{\partial S_e}\right)}{\frac{\partial f}{\partial \boldsymbol{\sigma}'} : \boldsymbol{C}^e : \frac{\partial f}{\partial \boldsymbol{\sigma}'} - \frac{\partial f}{\partial \varepsilon_v^p}\frac{\partial f}{\partial p'}} - K^{S_e}\mathbf{1}$$

For the soil–water characteristic curve model, this study uses the model introduced by Kawai et al. (2007), which enables the representation of hysteresis by using geometric similarity among scanning curves and which applies the following logistic curve equation proposed by Sugii and Uno (1996):

$$\frac{S_r - S_{ra}}{S_{rf} - S_{ra}} = \frac{1}{1 + \exp\left(A^\alpha + B^\alpha \log_e \frac{s}{s_0}\right)} \tag{14}$$

where S_{ra}: converging degree of saturation at $s \to 0$; S_{rf}: degree of saturation at $s \to 0$; A^α, B^α: shape parameters; and s_0: unit suction.

A.3. Governing Equations

Equation of motion: $\rho\ddot{\boldsymbol{u}} + \nabla \cdot \boldsymbol{\sigma} - \rho\boldsymbol{b} = 0$
Effective stress equation: $\boldsymbol{\sigma}' = \boldsymbol{\sigma}^{net} + p_s\mathbf{1}$
Constitutive equation: $\dot{\boldsymbol{\sigma}}' = \boldsymbol{C} : \dot{\boldsymbol{\varepsilon}} - \boldsymbol{D}\dot{S}_e$
Compatibility equation: $\boldsymbol{\varepsilon} = -\frac{1}{2}(\nabla \otimes \boldsymbol{u} + \boldsymbol{u} \otimes \nabla)$
Continuity equation (Solid-water): $-S_r\dot{\varepsilon}_v + n\dot{S}_r + \frac{nS_r}{K_w}\dot{p}_w + \mathrm{div}\tilde{\boldsymbol{v}}_w = 0$
Continuity equation (Solid-gas): $-(1-S_r)\dot{\varepsilon}_v - n\dot{S}_r + \frac{n(1-S_r)}{p_{a_0}+p_g}\dot{p}_g + \mathrm{div}\tilde{\boldsymbol{v}}_g = 0$
Darcy's law (Water): $\tilde{\boldsymbol{v}}_w = -\boldsymbol{K}_{\boldsymbol{w}}\nabla h = -k_{rw}\boldsymbol{k}_{\boldsymbol{w}}\nabla h$, $h = \frac{p_w}{\rho_w g} + h^e$
Darcy's law (Gas): $\tilde{\boldsymbol{v}}_g = -\boldsymbol{K}_{\boldsymbol{g}}\nabla h_g = -k_{rg}\boldsymbol{k}_{\boldsymbol{g}}\nabla h_g$, $h_g = \frac{p_g}{\rho_g g} + h_g^e$

In a quasi-static field, the equation of motion becomes an equilibrium equation because in that field the acceleration term is negligible. In these equations, ρ is the density of the entire region; $\boldsymbol{b}$ is the body force, ε_v is the volumetric strain; n is porosity; $\boldsymbol{u}$ is the displacement vector; $\dot{\boldsymbol{u}}$ is a velocity vector; $\ddot{\boldsymbol{u}}$ is an acceleration vector; $\boldsymbol{\sigma}$ is the total stress tensor; $\boldsymbol{\sigma}'$ is the effective stress tensor; $\mathbf{1}$ is the unit tensor; $\boldsymbol{\varepsilon}$ is the strain tensor; $\boldsymbol{C}$ is the elastic stiffness tensor; $\boldsymbol{D}$ is the coefficient tensor, p_w is the pore water pressure; p_g is the pore gas pressure; $\boldsymbol{k}$ is the hydraulic conductivity tensor; k_r is the specific hydraulic conductivity; h is the total head; h^e is the elevation head; g is acceleration due to gravity; and $\nabla = grad(\cdot) = \frac{\partial(\cdot)}{\partial \boldsymbol{X}}$ is the gradient operator in the reference configuration. Note that compression and tension are defined as positive and negative, respectively, as is customary in soil mechanics.

A.4. Boundary Conditions

Displacement boundary: $\dot{\boldsymbol{u}} = \bar{\dot{\boldsymbol{u}}}$ *on* S_u
Stress boundary: $\dot{\boldsymbol{\sigma}} \cdot \boldsymbol{n} = \bar{\dot{\boldsymbol{t}}}$ *on* S_σ
Head boundary (Water and gas, respectively): $h = \bar{h}$ *on* S_h
Flow rate boundary (Water and gas, respectively): $\tilde{\boldsymbol{v}}\boldsymbol{n} = \bar{q}$ *on* S_q

In these equations, $\boldsymbol{t}$ is the traction vector which acts on the boundary S_σ; $\boldsymbol{n}$ is the normal vector with respect to the boundary on which $\boldsymbol{t}$ acts; h is the total head; and q is the flow rate per unit area and time of flow in and out at boundary S_q. The bar ($\bar{}$) above the symbols denotes that it is a known parameter. Region V was created and its boundaries are defined as S ($S = S_\sigma + S_u = S_h + S_q$).

A.5. Initial Conditions

Initial stress: $\boldsymbol{\sigma}|_{t=0} = \bar{\boldsymbol{\sigma}}$
Initial head (Water and gas, respectively): $h|_{t=0} = \bar{h}$

A.6. Application to finite element method

To solve soil/water/gas coupled problems by the finite element method, weak formulations of the governing equations were made, or more specifically, the velocity equation of motion and the continuity equation, as shown in Appendix A.3, were differentiated in their respective regions using their respective arbitrary trial functions. For the spatial discretization (using the Galerkin method) of the governing equations that have undergone a weak formulation, isoparametric elements were used. Additionally, Gaussian integration was used to determine the accurate integral of an area. The spatially discretized equilibrium and continuity equations, respectively, were temporally discretized by the Euler method. The stiffness equation was obtained by using temporally discretized equilibrium and continuity equations.

References

Amaratunga, A., Grozic, J.L.H., 2009. On the undrained unloading behavior of gassy sands. Can. Geotech. J. 46 (11), 1267–1276.

Dietrich, G., 1963. General Oceanography. Interscience Publisher Inc., New York.

Esrig, Kirby, Robert C., 1977. Implications of gas content for predicting the stability of submarine slope. J. Mar. Geotechnol. 2(1)–(4), 81–100.

Fujishita, T., 1965. Rebound of saturated clay on removal of confinement pressure. Report of Port and Habour Technical Research Institute Ministry of Transportation, Japan 4(1) (in Japanese).

Grozic, J.L.H., Robertson, P.K., Morgenstern, N.R., 2000. Cyclic liquefaction of loose gassy sand. Can. Geotech. J. 37 (4), 843–856.

Hvorslev, M.J., 1949. Subsurface exploration and sampling of soils for civil engineering purposes. Water-Ways Experiment Station, Corps of Engineers, U.S, Army, 521p.

Kawai, K., Iizuka, A., Hayakawa, E., Wang, W., 2007. Non-uniform settlement of compacted earth structures caused by the deformation characteristics of unsaturated soil on wetting. Soils Found. 47 (2), 195–206.

Kawazu, J., Yasuhara, S., Kawai, K., Iizuka, A., 2011. The triaxial compression test with the smart triaxial apparatus. Report of Research Center for Urban Safety and Security, Kobe University, No. 15, 41–50 (in Japanese).

Kortekaas, S., Peuchen, J., 2008. Measured swabbing pressures and implications for shallow gas blow-out. Offshore Technology Conference, OTC19280.

Kubo, Y., Mizuguchi, Y., Inagaki, F., Yamamoto, K., 2014. A new hydro pressure-coring system for the drilling vessel Chikyu. Sci. Drill. 17, 37–43.

Ladd, C.C., Lamb, T.W., 1963. The strength of "undisturbed" clay determined from undrained testes, ASTM, STP-361(Laboratory Shear Testing of Soils), pp. 342–371.

Matsumoto, R., Okuda, Y., Hiruta, A., Tomaru, H., Takeuchi, E., Sanno, R., Suzuki, M., et al., 2009. Formation and collapse of gas hydrate deposits in high methane flux area of the Joetsu basin, Eastern margin of Japan Sea. J. Geogr. 118 (1), 43–71.

Matsumoto, K., Horie, H., Okumura, T., 1969. Studies on boring and sampling of saturated alluvial clays (4th Report). Report Port Harbour Research Institute 8 (2), 3–20 (in Japanese).

Matsuo, M., 1984. Geotechnical engineering. Principle and Practice of Reliability Design Method. GIHODO Press, pp. 28–31 (in Japanese).

Mitachi, T., Kudoh, Y., Tsushima, M., 2001. Estimation of in-situ undrained strength of soft soil deposits by use of unconfined compression test with suction measurement. Soils Found. 41 (5), 61–71.

Mualem, Y., 1976. A new model for predicting the hydraulic conductivity of unsaturated porous media. Water Resour. Res. 12 (3), 514–522.

Nakase, A., 1967. The $\varphi = 0$ analysis of Stability and Unconfined Compression Strength. Soils Found. 7 (2), 33–50.

Nishio, S., Hagisako, E., Denda, A., 2009. Geotechnical properties of core samples recovered from seabed ground in East Nankai Trough. J. Geogr. 118 (5), 955–968.

Noorany, I., Seed, H.B., 1965. In-situ strength characteristics of soft clays. J. Soil Mech. Found. Div. 91 (SM2), 49–80.

Ohno, S., Kawai, K., Tachibana, S., 2007. Elasto-plastic constitutive model for unsaturated soil applied effective degree of saturation as a parameter expressing stiffness. J. JSCE 63 (4), 1132–1141 (in Japanese).

Oka, T., Tanaka, H., Suzuki, K., Sakaiya, T., 2011. Characterization of soil properties during the filling process by CPT – a case study on the construction of the D-runway at the Tokyo International Airport. Jpn. Geotech. J. 6 (4), 489–501.

Okumura, T., 1969a. Studies on the disturbance of clay samples (2nd Report) – Stress changes of an unsaturated clay during sampling. Report Port Harbour Research Institute 8 (3), 77–98 (in Japanese).

Okumura, T., 1969b. Studies on the disturbance of clay samples (1st report) – remolding tests by the repeated triaxial compression. Report Port Harbour Research Institute 8 (1), 59–84 (in Japanese).

Okusa, S., 1984. Marine geotechnology – state-of-the-art. Jpn. Soc. Civ. Eng. 346, 13–21(in Japanese).

Skempton, A.W., 1954. The pore-pressure coefficients A and B. Géotechnique 4 (4), 143–147.

Skempton, A.W., Sowa, V.A., 1963. The behaviour of saturated clays during sampling and testing. Géotechnique 13 (4), 269–290.

Sugii, T., Uno, T., 1996. Modeling of hydraulic properties for unsaturated soils. Proc. Symp. Permeability of Unsaturated Ground, Japan, pp. 179–184 (in Japanese).

Sugiyama, Y., Kawai, K., Iizuka, A., 2016. Effects of stress conditions on B-value measurement. Soils Found. 56 (5), 848–860.

Tanaka, H., Sakakibara, M., Goto, K., Suzuki, K., Fukazawa, T., 1992. Properties of Japanese normally consolidated marine clays obtained from static piezocone penetration test. Report Port Harbour Research Institute 31 (4), 65–92 (in Japanese).

Tanaka, H., Tanaka, M., 1995. Sample quality by various types of samplers. Proc. of 10th ARCSMFE 1, 83–86.

Tanizaki, S., Oka, F., Kodaka, T., Kimoto, S., Watanabe, T., 2005. Cyclic elasto-viscoplastic constitutive modelling considering change of internal structure for naturally deposited clay. The Japan Society of Civil Engineers, Proc 60th Annual Meeting of JSCE (in Japanese).

Tsuchida, T., Kobayashi, M., Yamakawa, T., Taira, S., 1988. Effect of fissures on the undrained strength of clay. Report Port Harbour Research Institute 27 (1), 93–124 (in Japanese).

Tsui, Y., Helfrich, S., 1983. Wave-induced pore pressures in submerged sand layer. J. Geotech. Eng. 109 (4).

van Genuchten, M., 1980. A closed form equation for predicting the hydraulic conductivity of unsaturated soil. Soil Sci. Soc. Am. J. 44, 892–898.

Watabe, Y., Tsuchida, T., 2001. Influence of stress release on sample quality of Pleistocene clay collected from large depth in Osaka bay. Soils Found. 41 (4), 17–24.

Yamashita, S., Takahashi, N., Shoji, H., Minami, H., Hachikubo, A., Sakagami, H., Yamasaki, S., 2013. Survey report of sea bottom sediments off Abashiri, Okhotsk Sea (OS249 survey) (in Japanese).

Yamashita, S., Takahashi, N., Shoji, H., Minami, H., Hachikubo, A., Sakagami, H., Yamasaki, S., 2014. Survey report of sea bottom sediments off Abashiri, Okhotsk Sea (OS249 survey) (in Japanese).